ADVANCES IN INORGANIC CHEMISTRY, VOL. 33

CYSTEINE-CONTAINING OLIGOPEPTIDE MODEL COMPLEXES OF IRON–SULFUR PROTEINS

AKIRA NAKAMURA and NORIKAZU UEYAMA

Department of Macromolecular Science, Faculty of Science,
Osaka University, Toyonaka, Osaka 560, Japan

I. Introduction

Active centers of metalloproteins are presently better understood than ever before, and their unique properties are being further explored by application of modern techniques and theories of inorganic chemistry. Peptide environments exist around active centers and are thought to have significant control on their properties. Peptide sequence data are available which indicate that specific amino acids near the active centers dictate the spectroscopic as well as chemical reactivities.

The relationship between the structure of the peptide environment and active site chemical properties is thus of considerable interest and to a large extent awaits future studies. In this article, some examples of such specific relationships are described, particularly in the case of iron–sulfur proteins, because this class of proteins is distributed widely in living organisms ranging from bacterial cells to mammals. The major function of the proteins is now known to be electron transfer and the

redox catalysis associated with it. Here, iron–sulfur clusters are thought to play a decisive role in these biological electron transfer functions and the binding of such clusters is considered.

Extensive model studies on metal sulfide/thiolate complexes have already been performed. The work of Holm's group has been exemplary in the area of iron–sulfur proteins, and provides a sound basis for future studies (*1–3*). However, the nature of the ligands in simple model complexes of the iron–sulfur proteins, for example $[Fe(S_2\text{-}o\text{-}xyl)_2]^{-,2-}$ (S_2-*o*-xyl = *o*-xylene-α,α'-dithiolate), $[Fe_2S_2(S_2\text{-}o\text{-}xyl)_2]^{2-}$, and $[Fe_4S_4(SCH_2Ph)_4]^{2-}$, is not sufficiently precise to mimic the electron transfer properties of the native biological systems. Although such models reproduce many of the spectroscopic properties, the solubility, redox stability, and redox potentials have not as yet been adequately mimicked. Further studies are needed to meet these deficiencies and allow functionality to be related to the inorganic and biochemical components.

II. Significance of Peptide Ligands

A typical structure of a water-soluble globular protein consists of hydrophilic amino acid residues outside and hydrophobic ones inside. The hydrophobic environments support various electrostatic interactions within the protein, which plays a crucial role in the enzymatic reaction. Therefore, a simple model complex involving such electrostatic interactions must have hydrophobic environments around the active site such that they are not much influenced by an external effect of solvent. It follows that the models must to some extent be examined in a nonpolar solvent in order to mimic the behavior of native ones.

There are two types of metalloproteins containing cysteine residues as thiolate ligands. In one type, such as in aspartate carbamoyltransferase and alcohol dehydrogenase, M–S bonds serve as a connecting tool to maintain a tertiary structure of peptide chains. Figure 1 shows the basic geometries of the $[Zn(S\text{-}cys)_4]^{2-}$ cores in aspartate carbamoyltransferase and alcohol dehydrogenase (*4, 5*). These $[Zn(S\text{-}cys)_4]^{2-}$ units have D_{2d} or C_2 symmetry, respectively, although the ZnS_4 unit shows an almost regular T_d structure. Such a difference is caused by amino acid sequences. The two separate Cys-X-Y-Cys fragments chelate Zn(II) in D_{2d} symmetry and the Cys-X-Y-Cys-A-B-Cys fragment serves a C_2 structure, as shown in Fig. 2 (*4–7*). As a consequence of the chelation by peptide, the bond angles, especially M–S–CH_2–C dihedral angles, are restricted, and in some cases dis-

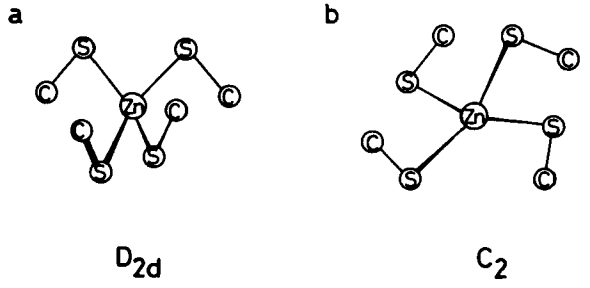

FIG. 1. The structure of ZnS_4 cores of (a) aspartate carbamoyltransferase (*4*) and (b) alcohol dehydrogenase [Zn(II)] (*5*).

torted coordination is observed. Such distortions seem to be important in the metallothioneins which have Cys-X-Cys or Cys-Cys fragments. The specific amino acid sequence is probably associated with peptide conformations suitable for formation of metal clusters, or for rapid ion-exchange between Zn(II) and Cd(II) (*8*); these are properties associated with the metallothioneins.

Another type of cysteine-containing metalloprotein which has M–S(cys) bonding at the active site is present in electron transfer proteins or metalloenzymes. Sulfur coordination is an important feature, and the covalency and "soft" environment are possible prerequisites for efficient electron transfer leading to redox catalysis. A distortion at the metal site is induced by the peptide ligands and is a significant feature of the active sites in metalloproteins containing transition metals Fe, Cu, Ni, Mo, etc.

Since the protein environment around the iron site of the iron–sulfur protein is related to the protein's biological function, peptide sequences nearest to the iron core are of utmost importance. Based on the peptide sequences reported for various iron–sulfur proteins, some examples of invariant sequences are discernible. For example, Cys-Gly-X-Cys sequences are involved in coordination at the active sites of bacterial ferredoxins (*9*). This macro-ring chelation is believed to be a feature and conveys specific chemical properties to the iron core.

Rubredoxin is a small protein which has one Fe ion (molecular weight 6000), as is schematically illustrated in Fig. 3. Jensen's group has revealed fairly precise structural features of the active site of *Clostridium pasteurianum* and *Desulfovibrio vulgaris* rubredoxins (*10, 11*). The simple model complex $[Fe(S_2\text{-}o\text{-}xyl)_2]^{-,2-}$ has been synthesized and analyzed crystallographically by Holm's group (*12*). Geometry of the FeS_4 core of the oxidized rubredoxin seems to be almost identical to that

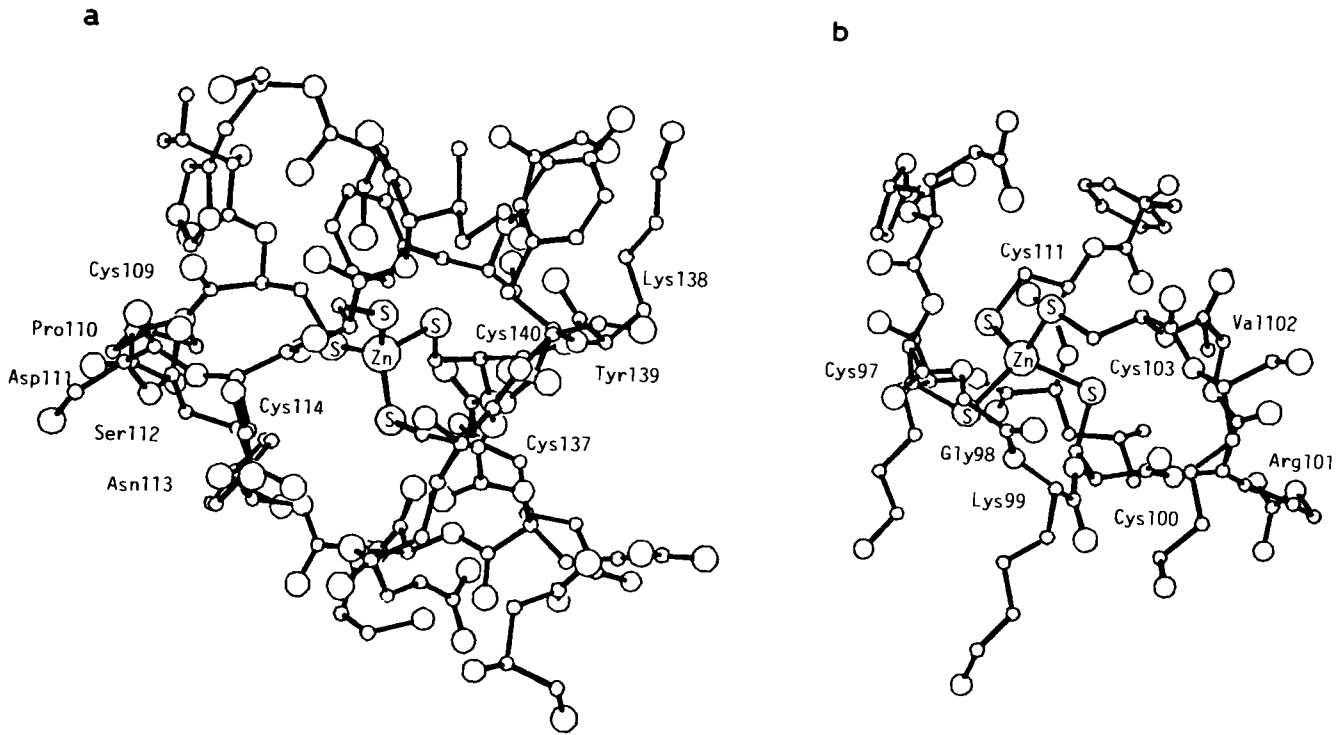

FIG. 2. The crystallographic structures of $Zn(S\text{-}cys)_4$ cores of (a) aspartate carbamoyltransferase ligated by Cys-Lys-Tyr-Cys and Cys-Pro-Asp-Ser-Asn-Cys (*4, 6*) and (b) alcohol dehydrogenase ligated by Cys-Gly-Lys-Cys-Arg-Val-Cys (*5, 7*). These illustrations are based on the X-ray crystallographic atomic coordinates listed in the Protein Data Bank.

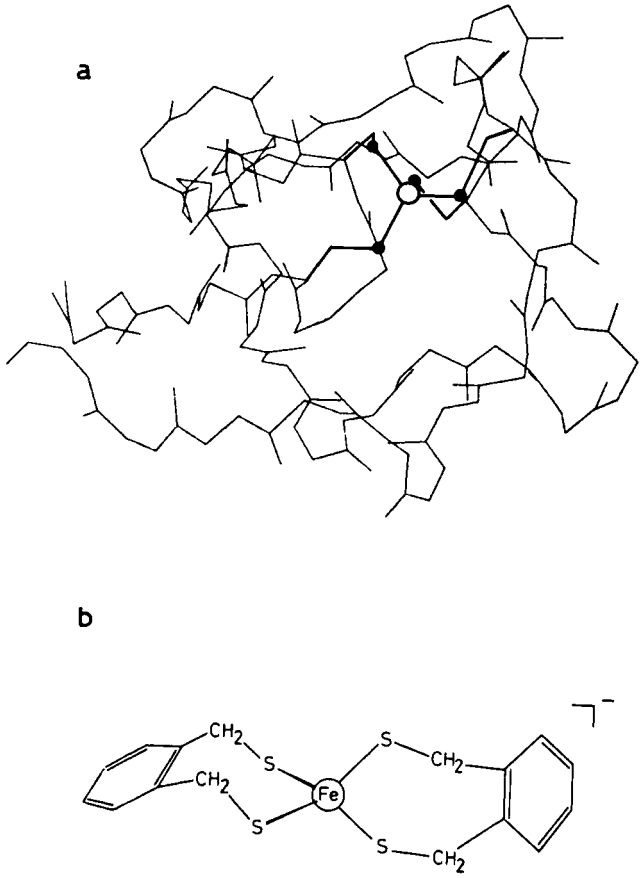

FIG. 3. The X-ray structures of (a) $Fe(S\text{-}cys)_4$ core and wire backbone peptide chain of *Desulfovibrio vulgaris* rubredoxin (the open circle and closed circles represent Fe and S atoms, respectively) (*6, 11*) and (b) $[Fe(S_2\text{-}o\text{-}xyl)_2]^-$ (*12*).

of $[Fe(S_2\text{-}o\text{-}xyl)_2]^-$. However, a large discrepancy between their redox potentials has been observed (*12*). The difference of approximately 0.3 V remains despite the theoretical correction made to allow for the replacement of solvent *N,N*-dimethylformamide (DMF) by aqueous solution. This point will be discussed in detail later. Important and critical differences in the electrochemical properties of simple synthetic model complexes and rubredoxin are, of course, due to the peptide environment around Fe ion, in this case the peptide chain Cys-X-Y-Cys. In order to clarify these differences one of fundamental approaches is to study oligopeptide complexes with ligands having the

same characteristic macro-ring peptide chelation as is found at the active site of the native protein. Invariant sections of amino acid sequences, particularly near the active site, are believed to control the specific chemical properties of the metal ions involved. Thus, oligopeptides having a similar sequence and a similar conformation to the native ones are important in model complexes.

There have been many attempts to synthesize model complexes of rubredoxin and ferredoxins using Cys-containing oligopeptides (*13, 14*). Unfortunately, synthetic methods for introduction of Fe(III) or $[Fe_2S_2]^{2+}$ into the peptides, or conditions to protect the $[Fe_4S_4]^{2+}$ core from hydrolysis, had not been established at that time of our initial research. Some relevant synthetic methods were developed mainly by Holm's group around 1974 (*15*). For example, most 4Fe–4S peptide complexes can be synthesized in solution by the ligand exchange reaction between a Cys-containing peptide and $[Fe_4S_4(S\text{-}t\text{-}Bu)_4]^{2-}$. Simple peptide ligands, i.e., Ac-Gly-Gly(Cys-Gly-Gly)$_2$NH$_2$, and their analogs have been examined as ligands to an $[Fe_4S_4]^{2+}$ core (*16*). The sequence Cys-Gly-Gly-Cys has a considerable amount of conformational freedom and does not seem to duplicate the characteristic effects of invariant sequences near the Fe core. Actually, this particular sequence has never been found in native iron–sulfur proteins. A systematic investigation is, therefore, necessary to establish a firm relationship between the peptide structure and the chemical functionality.

As a first step toward this purpose, we have studied the chelation effect of tetrapeptides of sequences Cys-X-Y-Cys, by preparation of metal complexes of mainly the first transition series. The hydrophobic effect of the peptides was also studied by utilizing the side chain bulkiness of the amino acid residues interposed between the two cysteine residues. A special effect of aromatic side chains of tyrosine, phenylalanine, and tryptophan has also been examined in order to assess their ability to ease electron transfer to and from the nearby iron core.

III. Chelating Effects of Peptide Ligands

A. Rubredoxin Peptide Model Complexes

Iron–sulfur proteins containing characteristic Cys-X-Y-Cys sequences have been found to exhibit enzymatic activity through an electron transfer. For example, rubredoxin has an Fe(II/III) ion surrounded by two Cys-X-Y-Cys sequences. Figure 4 shows a structure

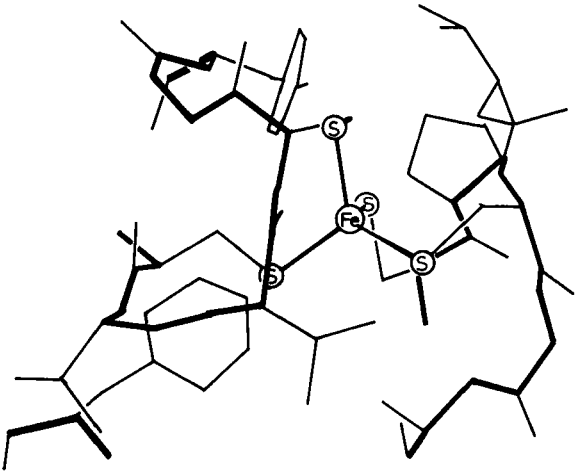

FIG. 4. The crystallographic structure within 5 Å of the active site of *Desulfovibrio vulgaris* rubredoxin (*6, 11*). Heavy lines represent peptide backbone chains.

within 5 Å of the active site of *D. vulgaris* rubredoxin by X-ray analysis (*11*). The FeS_4 core has a tetrahedral structure, as mentioned before, and the [Fe(S-cys)$_4$] core has an approximate D_{2d} structure similar to that of aspartate carbamoyltransferase. A simple synthetic model complex, $[Fe(S_2\text{-}o\text{-xyl})_2]^{-,2-}$, has been reported to have a C_2 symmetry, as shown in Fig. 3 (*12*). Native rubredoxin exhibits a reduction potential at -0.30 V versus SCE in aqueous solution for the Fe(III)/Fe(II) couple, while the same couple has a reduction potential of -1.0 V versus SCE in DMF. Other simple thiolate Fe(III) complexes with nonchelating ligands are thermally unstable, except for tetrakis(2,3,5,6-tetramethylbenzenethiolato)ferrate(III), which has bulky thiolate ligands (*17*).

The difference in redox potential and in thermal stability between native rubredoxin and the simple model complexes has been suggested to be brought about by the different "protein environments" (*18*). This is as yet unproved, however. The amino acid sequences of many rubredoxins isolated from various sources have been determined, as shown in Fig. 5 (*19*). A sequence around the Fe active site, Cys-X-Y-Cys, is an invariant fragment and primarily determines the chemical and physical properties. For example, *C. pasteurianum* rubredoxin has such sequences, Cys^6-Thr-Val-Cys^9 and Cys^{39}-Pro-Leu-Cys^{42}.

Studies of the synthesis of Fe(II) complexes of oligopeptides containing the two invariant Cys-X-Y-Cys fragments have been carried out to

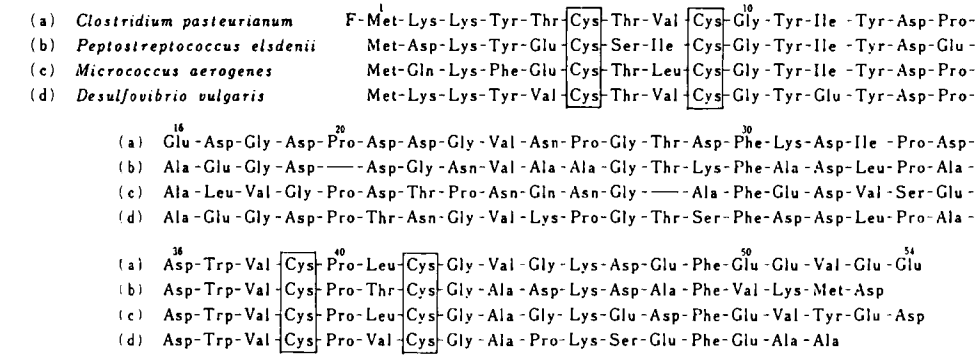

FIG. 5. Amino-acid sequences of various rubredoxins (*19*).

elucidate these differences. Because the Fe(II) thiolate bonding is ionic, and a dianionic $[Fe(S\text{-}cys)_4]^{2-}$ species exists, electrostatic interactions between the FeS_4 core and the peptide surround are important and may be enhanced by hydrophobic peptide environments. The hydrophobicity of peptide ligands may be simulated by an appropriate selection of the amino acid sequences. A systematic investigation by variation of the peptide sequence is of fundamental importance.

Table I lists the redox potentials of the Fe(II) peptide model complexes in Me_2SO (*20*). The model complexes of chelating peptides exhibit redox potentials for the Fe(II)/(III) couple in the range of -0.53 to -0.58 V versus SCE, which are remarkably positive compared

TABLE I

THE REDOX POTENTIALS OF THE Fe(II)/L-L PEPTIDE MODEL COMPLEXES IN Me_2SO

Complex	Redox potential (V versus SCE)
Z-Cys-Pro-Leu-Cys-OMe	-0.54
Z-Cys-Thr-Val-Cys-OMe	-0.53
Z-Cys-Ala-Ala-Cys-OMe	-0.58
Z-Cys-Ala-Cys-OMe	-0.55
S_2-*o*-xyl	-0.98[a]

[a] Isolated $[Fe(S_2\text{-}o\text{-}xyl)_2]^-$ was reported to exhibit a redox potential at -0.98 V versus SCE in Me_2SO (*12*).

with the value (-0.98 V versus SCE in Me_2SO) for $[Fe(S_2\text{-}o\text{-}xyl)_2]^-$. The chelation of the Cys-X-Y-Cys peptides is thus an important factor, which forces the peptide chain to form NH---S hydrogen bonds with a preferable conformation.

The redox stability of the various model complexes was examined in aqueous Triton X-100 solutions. Only $[Fe(Z\text{-}cys^1\text{-}Pro\text{-}Leu\text{-}cys\text{-}OMe)_2]^{2-}$ exhibits a quasireversible redox couple at -0.37 V versus SCE, which is considered to simulate closely the value of native rubredoxin, although a small difference (0.1 V) still remains (*7*). Other model peptide complexes are rapidly decomposed by hydrolysis in an aqueous micellar solution and do not exhibit even an oxidation peak. The simple alkythiolate model $[Fe(S_2\text{-}o\text{-}xyl)_2]^{2-}$ exhibits a quasireversible redox couple at -1.0 V versus SCE in an aqueous micellar solution. Therefore, macro-ring peptide chelation with some hydrophobic side chains, is required in order to induce redox stability (reversibility of cyclic voltammogram measurements) of the Fe(III/II) couple.

The X-ray structure reported for the Cys-Pro-Val-Cys and Cys-Thr-Val-Cys sequences in *D. vulgaris* rubredoxin (*7, 10*) suggests that the alkyl and alkylene side chains of the Cys-Pro-Val-Cys or Cys-Pro-Leu-Cys fragment protect the NH---S hydrogen bonds as shown in Fig. 6. The NH---S hydrogen bonds in Cys-Thr-Val-Cys are effectively protected from the polar solvents by a phenyl group of a remote amino acid residue. In the synthetic model, however, no phenyl group is available for the protection. Thus, the difference in stability against hydrolysis between $[Fe(Z\text{-}cys\text{-}Pro\text{-}Leu\text{-}cys\text{-}OMe)_2]^{2-}$ and $[Fe(Z\text{-}cys\text{-}Thr\text{-}Val\text{-}cys\text{-}OMe)_2]^{2-}$ is ascribed to the protection of the $[Fe(SR)_4]^{2-}$ core by the hydrophobic side chains and to the formation of the NH---S hydrogen bonds by taking a specific conformation in an aqueous micellar solution.

The specific NH---S hydrogen bonding is considered to contribute to elongation of the Fe–S bond by weakening the bond. The Fe–S bonds of the two Cys thiolates at the N terminals of the tetrapeptide ligands should be affected because Cys^1-X-Y-Cys^4 chelates to the Fe, and only NH groups of Y and Cys^4 can form NH---S hydrogen bonds to the Cys^1 sulfur (Fig. 7b).

In order to estimate the effect of NH---S hydrogen bonding in shifting redox potentials, extended Hückel MO calculations have been carried out for the D_{2d} geometry of $[Fe(SCH_3)_4]^-$ (Fig. 7a) (*21*). Thus, the overlap populations of four Fe–S bonds have been obtained by varying the two Fe–S(Cys^1) bond lengths in the Cys-X-Y-Cys/Fe(III) complex. The energy level of the singly occupied b_1 orbital was found to

[1] Lowercase cys refers to the amino acid residue involved in coordination.

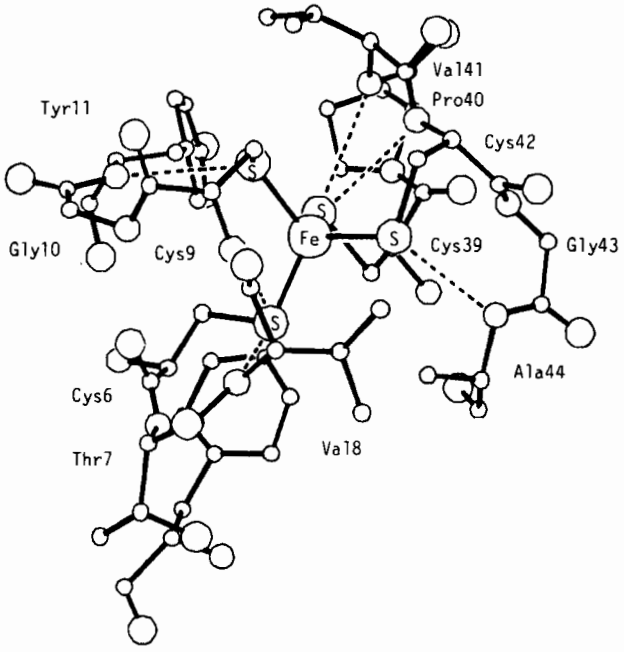

FIG. 6. NH---S hydrogen bonds (dashed lines) in Cys-Pro-Val-Cys-Gly-Ala and Cys-Thr-Val-Cys-Gly-Tyr fragments in *Desulfovibrio vulgaris* rubredoxin (*6, 11, 20*).

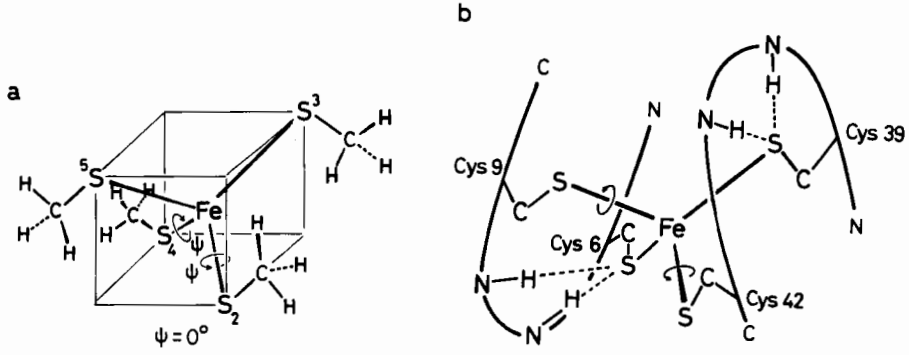

FIG. 7. (a) The idealized geometry of a model $[Fe(SCH_3)_4]^-$ used for the extended Hückel calculations and (b) schematic presentation of the proposed structure for $[Fe(Z\text{-cys-X-Y-cys-OMe})_2]^-$ or native rubredoxin (*21*).

decrease with the elongation of the Fe–S bond. Therefore, the elongation is considered to contribute to the positive shift of the redox potential of $[Fe(Z\text{-cys-X-Y-cys-OMe})_2]^{2-/-}$.

The crystal structure of oxidized *C. pasteurianum* rubredoxin has been analyzed up to 1.2 Å refinement by Jensen's group (*10, 22, 23*). The values of Fe–S bond lengths obtained from extended X-ray absorption fine structure (EXAFS) analysis (*24*) correspond well to those from the crystallographical analysis (*23*). These studies have concluded that the $Fe(S\text{-cys})_4$ core with equal Fe–S bond lengths has an approximate D_{2d} structure. Table II shows the four Fe–S Raman stretching bands of $[Fe(S_2\text{-}o\text{-xyl})_2]^-$, and those of oxidized *Desulfovibrio gigas* rubredoxin (*25, 26*). Spiro *et al.* found that distortion of the angle split the T_2 mode for the model complex and the protein. They have observed four resonance Raman bands with Fe–S stretching vibrations at 314, 348 (shoulder), 363, and 376 cm^{-1} for *D. gigas* oxidized rubredoxin, which was also established by the Raman spectra of ^{54}Fe-substituted rubredoxin (*26*). They also found an appreciable effect of the S–C dihedral angles on the Fe–S breathing mode. This effect accounts for the frequency difference between oxidized rubredoxin and the analog complex, $[Fe(S_2\text{-}o\text{-xyl})_2]^-$. The constancy of ν(Fe–S) bands in *D. gigas, Desulfovibrio sulfuricans*, and *Megasphera elsdenii* was interpreted to imply that the same set of Fe–S–CH_2–C dihedral angles are different from those of $[Fe(S_2\text{-}o\text{-xyl})_2]^-$.

Besides the NH---S hydrogen bonding, an effect of chelation is expected to arise from the variation of Fe–S torsion angles. The presence of this effect was suggested from the ^{1}H NMR data of $[Fe_2S_2(Z\text{-cys-X-Y-cys-OMe})_2]^{2-}$, where Z-Cys-X-Y-Cys-OMe (Z and OMe are substituents at the Cys residues) provides two contact-shifted

TABLE II

RAMAN BANDS (cm^{-1}) OF Fe–S VIBRATIONS OF TETRAHEDRAL Fe(III) THIOLATO COMPLEX AND NATIVE RUBREDOXIN

Assignment	$[Fe(S_2\text{-}o\text{-xyl})_2]^{-}$ [a]	Rd_{ox} [a]	Rd_{ox} [b]
Fe–S I	297	312	314
Fe–S II	321	325	348
Fe–S III	350	359	363
Fe–S IV	374	371	376

[a] Ref. (*25*).
[b] Ref. (*26*).

peaks of the Cys CH_2 at 30.7 and 22.9 ppm in Me_2SO-d_6 (*27*). On the other hand, $[Fe_2S_2(Z\text{-cys-X-OMe})_4]^{2-}$ with a nonchelating peptide ligand exhibits one contact-shifted peak at 30.7 ppm for Cys CH_2. The difference is due to the characteristic chelation of the peptide to an Fe(III) ion besides the formation of NH---S hydrogen bond.

The chelation effect of Cys-X-Y-Cys was also found for the MCD spectra of Fe(III) complexes of Z-Cys-Pro-Leu-Cys-OMe or Z-Cys-Ala-Ala-Cys-OMe, which exhibited a characteristic ligand–metal charge transfer (LMCT) at 350 nm, but not for those of the Fe(III) complex of Z-Ala-Cys-OMe, Z-Cys-Ala-Cys-OMe, or S_2-*o*-xyl (*28*). The MCD spectral differences in the region of 300–400 nm are related to the difference in the electronic states of the Fe(III) singly occupied metal t_2 orbitals affected by the lone pair on the sulfur atom. The possibility of a spectroscopic splitting by a specific Cys–thiolate orientation relative to other Fe–S bondings has been predicted theoretically by Bair and Goddard (*29*). The orientation of π orbitals of the sulfur lone pair is now found to be determined by the peptide conformation which dictates the steric disposition of the S–C bond.

The chelation effect also brings about a stabilization of the -1 state of the peptide model complexes as indicated by the thermal stability and redox behavior. Only $[Fe(Z\text{-cys-Pro-Leu-cys-OMe})_2]^-$ exhibits a relatively reversible redox couple in the cyclic voltammogram measurement, but the others do not (*20*). The bulkiness of side chains of the X and Y residues in Cys-X-Y-Cys probably restricts the adoption of the inherent by preferable conformation ($\psi = 0°$), resulting in a more restricted orientation of Fe–S–C. In fact, the X-ray analysis of native rubredoxin shows that two of the Fe–S torsion angles are restricted and the other two are normal, i.e., conformationally more stable.

An MO calculation was performed varying the S–Fe–S–CH_3 dihedral angle (Fe–S torsion angle). For example, two Fe–S bonds of $[Fe(SCH_3)_4]^-$ were rotated in the same direction. Because a synthetic model, $[Fe(Z\text{-cys-Pro-Leu-cys-OMe})_2]^{-,2-}$, has two symmetrical Cys^1-X-Y-Cys^4 sequences, either of the torsion angles of the two Fe–S bonds of the Cys^1 and Cys^4 residues is considered to be restricted by the bulkiness of the side chains in the X–Y sequence.

The overlap population of Fe–S bonds was found to be explicitly dependent on the two torsion angles of Fe–S. The Fe–S torsion angle dependence of the overlap populations with variation of the two Fe–S torsion angles is shown in Fig. 8. The increase in the overlap populations for two restricted Fe–S bonds is reflected by the experimental data of shortening the Fe–S bond, whereas the other two Fe–S bonds having the normal torsion angle show the decrease in the overlap

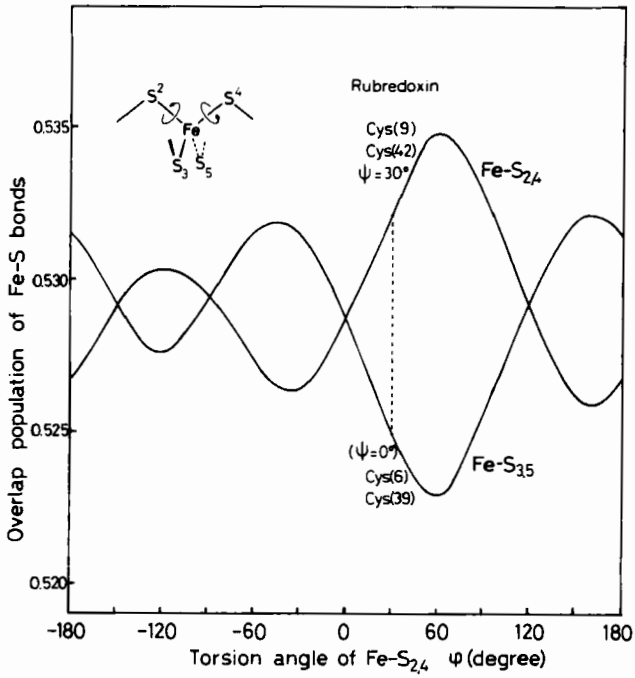

FIG. 8. Variation of the overlap population of Fe–S bonds with two Fe–S torsion angles (all Fe–S bond lengths are fixed in 2.29 Å). (Reproduced by permission of the American Chemical Society.)

populations. This theoretical prediction refers to the elongation of Fe–S bond length. Actually, the extended Hückel MO calculation data are consistent with the parameters of Fe–S bond lengths and Fe–S–C bond angles (Table III) in Cys^{6}-X-Y-Cys^{9} or Cys^{39}-X-Y-Cys^{42} obtained by the X-ray analysis of *C. pasteurianum* rubredoxin (*10, 22*). The Fe–S bonds of Cys^{6} and Cys^{39} are long with small Fe–S–C angles, whereas the Fe–S bonds of Cys^{39} and Cys^{42} are short with large Fe–S–C angles. Thus, by formation of the angularly restricted Fe–S bonds, the bonds become ionic in character, resulting in the stabilization of the Fe(III) state.

B. [2Fe–2S] PLANT-TYPE FERREDOXIN PEPTIDE MODEL COMPLEXES

The structure of oxidized *Spirulina platensis* ferredoxin has been established by X-ray analysis, and is as shown in Fig. 9 (*30*). Three Cys thiolates in an invariant sequence, Cys-A-B-C-D-Cys-X-Y-Cys, bind the

TABLE III

Fe–S Bond Lengths and Fe–S–C Angles of the Active Site of *Clostridium pasteurianum* Rubredoxin with 1.2-Å Refinement X-Ray Analysis

Fe–S bond lengths[a] (Å)	Cys6	2.33(1)
	Cys9	2.29(1)
	Cys39	2.30(1)
	Cys42	2.24(1)
Fe–S–C angles[a] (degrees)	Cys6	100.1(4)
	Cys9	107.8(4)
	Cys39	99.3(4)
	Cys42	109.5(4)

[a] Ref. (*10*).

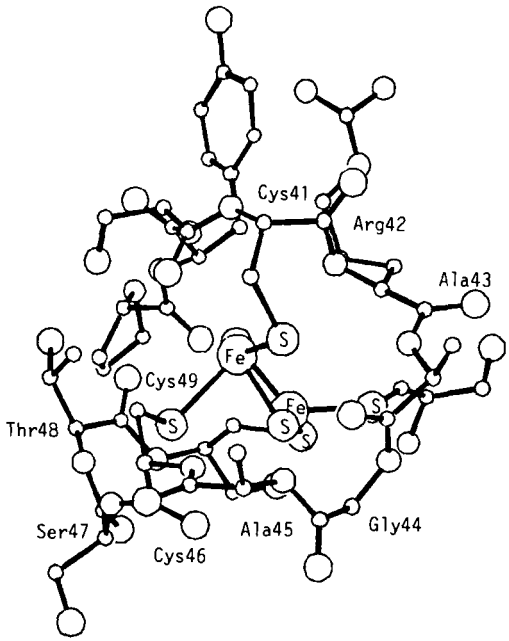

FIG. 9. The X-ray structure within 5 Å of Fe_2S_2 core ligated by Cys-Arg-Ala-Gly-Ala-Cys-Ser-Thr-Cys is *Spirulina platensis* ferredoxin (*6, 30*).

binuclear $Fe_2S_2^{2+}$ core. The presence of many NH---S hydrogen bonds has been speculated by the distances and the orientations of the N and S atoms. Recently, the presence of NH---S hydrogen bond has been supported by studies using resonance Raman spectroscopy (*31*). The precise value of the redox potential of the plant-type ferredoxin is crucial in the construction of an electron transfer chain in biological photosynthesis. Spinach ferredoxin has a redox couple at -0.64 V versus SCE in aqueous solution which is relatively positive compared to that of model complexes (*32*). The position of this redox potential is believed to be optimal for the *in vivo* systems. Synthetic model complexes, however, have considerably negative redox potentials, for example, -1.49 V versus SCE in DMF for $[Fe_2S_2(S_2\text{-}o\text{-xyl})_2]^{2-}$ (*33*) and -1.06 V versus SCE in DMF for $[Fe_2S_2(\text{Z-cys-Ala-Ala-cys-OMe})_2]^{2-}$ (*27*). Furthermore, the peptide model complexes $[Fe_2S_2(\text{Ac-Gly-Gly-(cys-Gly-Gly)}_2\text{NH}_2)_2]^{2-}$ (*34*) and $[Fe_2S_2(\text{Z-cys-Ala-Ala-cys-OMe})_2]^{2-}$ (*27*), which were synthesized from $[Fe_2S_2Cl_4]^{2-}$ and the corresponding oligopeptide, show two characteristic absorption maxima similar to those of native plant-type ferredoxins, but somewhat shifted. Thus, the modification of electrochemical and spectrochemical properties are considered to be due to an unidentified interaction between the peptide and the $Fe_2S_2^{2+}$ core. Simple model complexes do not duplicate the crucial function of the native proteins and further elaboration at the peptide ligand structure is necessary.

In order to find an essential sequence which provides the positive shift of the redox potential, various Cys-containing oligopeptide [2Fe–2S] model complexes were synthesized by our group. For example, the nature of the chelate ring in $[Fe_2S_2(\text{Z-cys-Ala-Ala-cys-OMe})_2]^{2-}$ was examined. Titration with 3,4-toluenedithiol indicated that Z-Cys-Ala-Ala-Cys-OMe chelates to one Fe(III) ion, and Cys-X-Y-Cys is not involved in bridging between two Fe(III) ions, as has been found in native plant-type ferredoxins (*34*). The ligand exchange reaction of Eq. (1) was confirmed by the determination of the released hydrogen

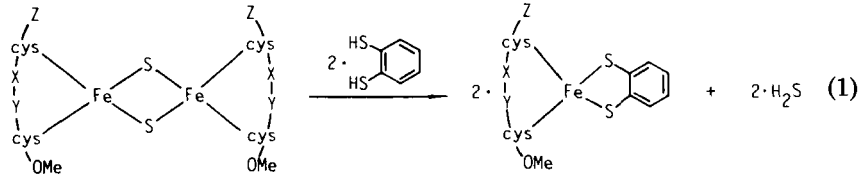

(1)

sulfide. The peptide complex $[Fe_2S_2(\text{Z-cys-X-Ala-Gly-Ala-cys-OMe})_2]^{2-}$ (X = Gly or Ala) further confirms that the conformationally preferable

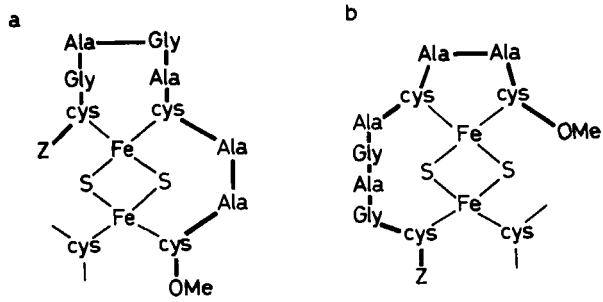

FIG. 10. The proposed two isomers of $[Fe_2S_2$(Z-cys-Gly-Ala-Gly-Ala-cys-Ala-Ala-cys-OMe)(Z-Val-cys-Val-OMe)$]^{2-}$ in DMF (*35*). *Spirulina platensis* ferredoxin has structure a.

coordination is chelation to one Fe(III) ion (*35*). In the case of the $[Fe_2S_2$(Z-cys-Gly-Ala-Gly-Ala-cys-Ala-Ala-cys-OMe)(Z-Val-cys-Val-OMe)$]^2$ complex, two redox couples are observed due to the existence of two isomers (*35*). One of the two redox couples was observed at -0.94 V versus SCE in DMF or at -0.81 V versus SCE in acetonitrile. This form is believed to have the same structure as that of native plant-type ferredoxin. Thus, Cys-X-Y-Cys in the Cys-A-B-C-D-Cys-X-Y-Cys peptide competes with Cys-A-B-C-D-Cys for chelation to one Fe(III) ion of $Fe_2S_2^{2+}$ core as shown in Fig. 10. The solvent dependence of the redox potential can be assigned to NH---S hydrogen bond formation in the less strongly solvating acetonitrile. Thus, the formation of NH---S hydrogen bonds affects the electrochemical properties of the $[Fe_2S_2(SR)_4]^{2-}$ core. It is concluded that the positive shift in redox potential is the result of a combination of NH---S hydrogen bonding and the conformation adopted by the peptide.

C. [3Fe–xS] FERREDOXINS

Azotobactor vinelandii ferredoxin I has two Fe/S clusters, [4Fe–4S] and a [3Fe–xS], with redox potentials at -0.42 and $+0.32$ V versus NHE, respectively (*36*). The existence of a normal $Fe_4S_4^{2+}$ core and a [3Fe–3S](S-cys)$_5$(oxo) core has been considered. In the ferredoxin I the unique sequence Cys-Val-Glu-Val-Cys has been suggested as a tridentate ligand for the [3Fe–3S] cluster (*37*). Recently, the structure has been crystallographically (*38*) corrected, and the iron–sulfur centers are now believed to consist of $Fe_4S_4^{2+}$ and [3Fe–4S] clusters, as proposed by EXAFS (*39*). One possibility is that the above-mentioned [3Fe–xS] structure is formed during isolation by oxidative removal of an Fe ion from the [4Fe–4S] cluster (*40*).

$Fe_4S_4^{2+}$ and [3Fe-xS] clusters have also been identified in *Pseudomonas ovalis* ferredoxin using the ^1H NMR spectral method (*41*). Again it is claimed that the [3Fe–4S] cluster is formed from [4Fe–4S] during the purification procedures. Such a process has also been observed in aconitase, which has only a simple Fe/S cluster (*42*).

No [3Fe–4S] peptide model complexes have been reported although such incomplete cuboidal complexes are important as starting material in the synthesis of other relevant complex cuboidal containing transition metal ions such as Mo or Ni ions.

D. [4Fe–4S] FERREDOXIN PEPTIDE MODEL COMPLEXES AND MODEL REACTIONS

Simulation of redox potentials for the $-3/-2$ couples of the synthetic $[Fe_4S_4(SR)_4]^{2-}$ complexes, such as $[Fe_4S_4(S\text{-}p\text{-}NO_2\text{-}Ph)_4]^{2-}$ (*43*) and $[Fe_4S_4(t\text{-}Boc(Gly\text{-}Cys\text{-}Gly)_3NH_2)(S\text{-}t\text{-}Bu)]^{2-}$ (*16*), have already been achieved. The values obtained are similar to those of bacterial ferredoxins, which have the most negative redox potentials among many native ferredoxins. An approach has been made to control the redox potential by substitution of an electron-donating or electron-withdrawing group on the benzenethiolate ligands of the Fe_4S_4 core. Another factor for the positive shift of redox potential is associated with a peptide ligand. Que *et al.* have found that the positive shift of $-3/-2$ redox potentials can be ascribed to the increase in the dielectric constant of the solvent surrounding the ferredoxin model complex. This effect was theoretically supported by Kassner and Yang (*44*). However, a more positive shift by other extrinsic factors is required in order to attain the redox potentials of native ferredoxins. An investigation or the effect of a peptide environment around the $Fe_4S_4^{2+}$ core should be considered in this respect.

The spectral and electrochemical properties of the $Fe_4S_4^{2+}$ complexes of Cys-containing oligopeptides having an invariant sequence of bacterial ferredoxins have been studied. One of the characteristic features of the peptide ligand is its ability to form hydrogen bonds between amide groups and coordinating sulfur atoms. The presence of many NH---S hydrogen bonds has been proposed in the X-ray analysis of *Pseudomonas aerogenes* ferredoxin (Fig. 11) (*45*). A theoretical prediction for the presence of NH---S hydrogen bonds has been obtained by *ab initio* calculations (*46*). The precise chemical roles of NH---S hydrogen bonds were examined using synthetic peptide model complexes. The change of redox potentials (-0.84 V versus SCE at $-40°C$; -0.99 V versus SCE at 31°C) for $[Fe_4S_4(Z\text{-}cys\text{-}Gly\text{-}Ala\text{-}OMe)_4]^{2-}$ due to

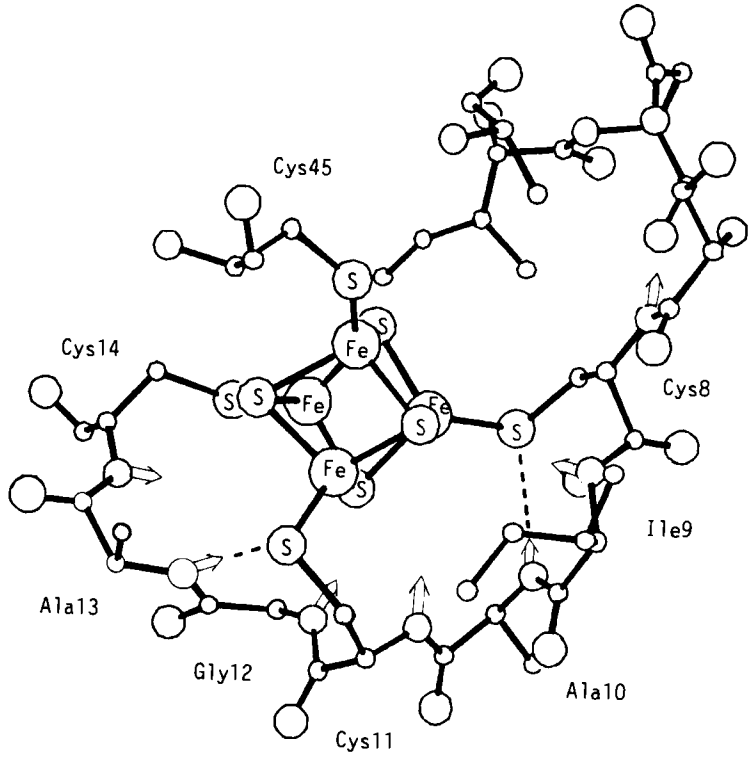

FIG. 11. The crystallographic structure within 5 Å of the Fe_4S_4 cluster I ligated by Cys-Ile-Ala-Cys-Gly-Ala-Cys in *P. aerogenes* ferredoxin (*6, 43*). Open arrows show the direction of NH groups.

NH---S hydrogen bonding is supported by measurements in a low dielectric solvent such as dichloromethane (*47*). However, the difference from the dielectric constants of DMF and dichloromethane is negligible, and it is likely therefore that the NH---S hydrogen bonds are stabilized in dichloromethane by the conformational freezing of Z-Cys-Gly-Ala-OMe at the lower temperature, as shown in Fig. 12. The stronger solvation of DMF results in disruption of the NH---S hydrogen bonds.

The preferential formation of NH---S hydrogen bonding in less polar solvents is also supported by the results of the solvent dependence of the LMCT absorption maxima of $[Fe_4S_4(Z\text{-cys-Gly-Ala-OMe})_4]^{2-}$ or $[Fe_4S_4(Z\text{-cys-Gly-OMe})_4]^{2-}$. The former complex has maxima at 406 nm in DMF and 390 nm in dichloromethane, but the latter complex shows absorption maxima at 402 nm in DMF and 402 nm in dichloromethane. Absence of the effect of the hydrogen bonding in the complex with Z-Cys-Gly-OMe is evident.

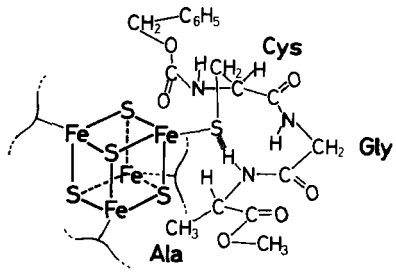

FIG. 12. The proposed structure of $[Fe_4S_4(Z\text{-cys-Gly-Ala-OMe})_4]^{2-}$ in dichloromethane (*45*).

Generally, $[Fe_4S_4(SR)_4]^{2-}$ in a high-dielectric-constant solvent, such as water, provides a blue shift of the LMCT absorption maximum. Therefore, the unusual blue shift of the LMCT absorption maximum in less polar solvent, such as dichloromethane, is ascribed to a strong interaction of the $[Fe_4S_4(SR)_4]^{2-}$ cluster with the NH group of the Ala. The above-mentioned conformational freezing of Z-Cys-Gly-Ala-OMe at low temperature was also confirmed by the temperature and solvent dependencies of IR and CD spectra of $[F_4S_4(Z\text{-cys-Gly-Ala-OMe})_4]^{2-}$ in dichloromethane (*47*). It should be emphasized that an electrostatic interaction such as that in NH---S hydrogen bonding is facilitated in nonpolar solvent. Thus, the importance of such enhanced electrostatic interactions has been generally recognized in the active sites of proteins (*48*).

Two peptide model complexes containing the invariant sequence Cys-X-Y-Cys have been synthesized. A remarkable positive shift of the redox potential of $[Fe_4S_4(Z\text{-cys-Gly-Ala-cys-OMe})_2]^{2-}$ in dichloromethane was found at $-43°C$, just as was observed for $[Fe_4S_4(Z\text{-cys-Gly-Ala-OMe})_4]^{2-}$, although $[Fe_4S_4(Z\text{-cys-Ile-Ala-cys-OMe})_2]^{2-}$ exhibits no such temperature dependence. On the contrary, in DMF, both complexes showed no temperature dependence of the redox potentials from -40 to $30°C$ (*49*). The chelation by Cys-X-Y-Cys supports the formation of NH---S hydrogen bonds when the macro-ring has a suitable conformation. Such a chelation has been found for the bidentate ligand of Cys-X-Cys in $[Fe_4S_4(Z\text{-cys-Gly-cys-NH-Ph})_2]^{2-}$ (*50*). Furthermore, the presence of a Gly residue adjacent to the Cys thiolate was found to be advantageous, giving a preferable conformation leading to NH---S hydrogen bonding. Introduction of an Ile instead of Gly residue next to the Cys residue resulted in a negative shift of the reduction peak and lower stability of the -3 state in the case of $[Fe_4S_4(Z\text{-cys-Ile-Ala-OMe})_4]^{2-}$. As shown in Fig. 13, the peptide fragment,

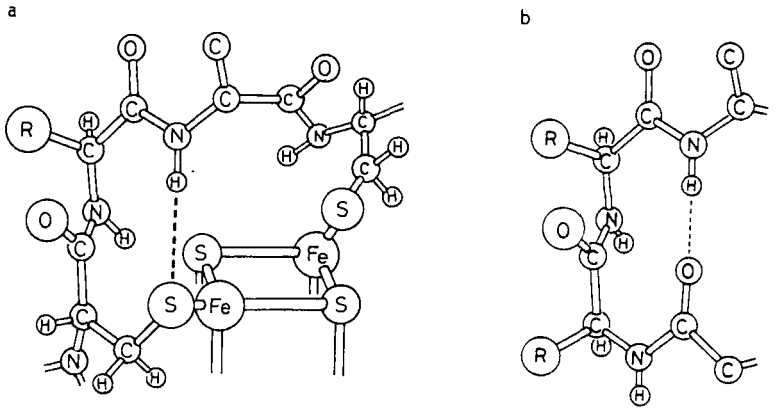

FIG. 13. (a) β-Turn conformation of the Cys-X-Y-Cys fragment coordinating to the $Fe_4S_4^{2+}$ core and (b) β-II hairpin turn conformation of a tetrapeptide fragment.

Cys-Gly-Ala provides a β-II like conformer with NH---S hydrogen bonding. Bulkiness of a substituent R group on an amino acid residue adjacent to the Cys residue prevents the Ala NH group from forming NH---S hydrogen bonds (*45, 47*). Consequently, it is concluded that the identity of the amino acid residues following the coordinated cysteine residue controls the electrochemical as well as the spectroscopic properties of the [4Fe–4S] core.

The simple peptide ligand Cys-Gly-Gly-Cys-Gly-Gly-Cys, when coordinated to an Fe_4S_4 core, is believed to give two isomers because of its tridentate coordination geometry and the absence of effective conformational restriction by the Gly residues, as shown in Fig. 14 (*16*). Further studies on heptapeptide complexes containing three Cys

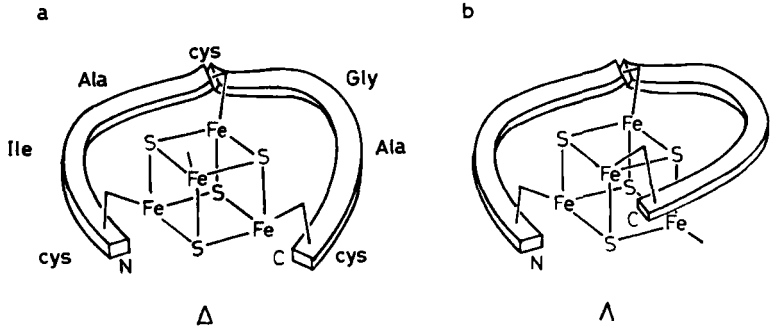

FIG. 14. The proposed (a) favorable, Δ, and (b) unfavorable, Λ, isomers of tridentate peptide complexes with nonbulky amino acid residues (*16*).

residues, e.g., $[Fe_4S_4(Z\text{-cys-Ile-Ala-cys-Gly-Ala-cys-OMe})(S\text{-}t\text{-Bu})]^{2-}$, were carried out, because the sequence represents an invariant one around the active site of bacterial ferredoxins. However, the complex exhibits three redox couples in the $-3/-2$ region due to the existence of at least three isomers, which probably have different coordination states, as illustrated in Fig. 15 (*51*). The Cys CH_2 region in the ^1H NMR spectra of the synthetic heptapeptide complexes is similar to those of *P. aerogenes* ferredoxins (*52*). A highly contact-shifted CH_2 signal was observed at 17 ppm which is very similar to that of native *P. aerogenes* ferredoxin. The signal due to one of the three Cys CH_2 groups in the tridentate ligand Cys^1-X-Y-Cys^4-A-B-Cys^7 is highly contact shifted, depending presumably on the Fe–S bond character, and gives the peak at 17 ppm. Thus, the heptapeptide complex probably has a structure similar to that of the native protein.

The heptapeptide complex exhibits a redox potential at -0.80 V versus SCE in dichloromethane and at -0.78 V versus SCE in DMF at room temperature. Such positive-shifted redox potentials in various organic solvents at room temperature provides an important insight into the control mechanism at the active site of [4Fe–4S] ferredoxins.

The model complex $[Fe_4S_4(Z\text{-cys-Ile-Ala-cys-Gly-Ala-cys-OMe})(Z\text{-cys-Pro-Val-OMe})]^{2-}$ was synthesized and had all amino acid residues within 5 Å from the $Fe_4S_4^{2+}$ core in cluster I of *P. aerogenes* ferredoxin (*51*). The complex had a redox potential at -0.88 V versus SCE in DMF and -0.83 V versus SCE in dichloromethane. In this case only one isomer was detected by cyclic voltammetry. For these complexes, a lesser degree of solvent dependence was found in the LMCT absorption maxima and in the redox potentials. This is due to the fact that the $[Fe_4S_4(SR)_4]^{2-}$ cluster is well shielded from solvent by the combined steric bulk of the Z-Cys-Ile-Ala-Cys-Gly-Ala-Cys-OMe

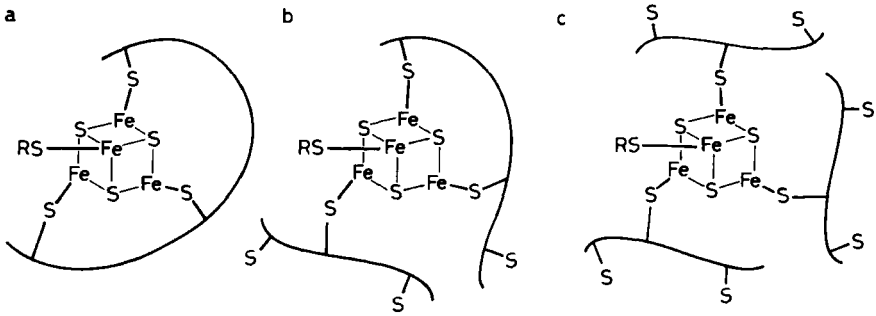

FIG. 15. Three types of the proposed isomers containing Z-Cys-Ile-Ala-Cys-Gly-Ala-Cys-OMe, which binds $Fe_4S_4^{2+}$ as (a) tridentate, (b) bidentate, or (c) monodentate.

and Z-Cys-Pro-Val-OMe ligands. Thus, it is likely that the redox potential of ferredoxin is mainly defined by the chemical environments of the amino acid residues present in the invariant sequences within 5 Å from the $Fe_4S_4^{2+}$ core.

IV. Hydrophobic Effect of Peptide and Related Ligands

A hydrophobic environment around the iron site has been found to exist on the inside of many globular proteins. In the case of HiPIP, an Fe_4S_4 is buried in the hydrophobic cavity of the protein. The local structure within 5.5 Å of the core shows the situation more clearly, as shown in Fig. 16 (*53*). Especially noticeable here are the Trp side chains, which originate from a characteristic peptide sequence of Trp-Cys or Trp-Cys-Ala at the coordinating cysteine residues. We have examined the effect of Trp by preparation and spectroscopic and electrochemical measurements of its Fe_4S_4 complexes.

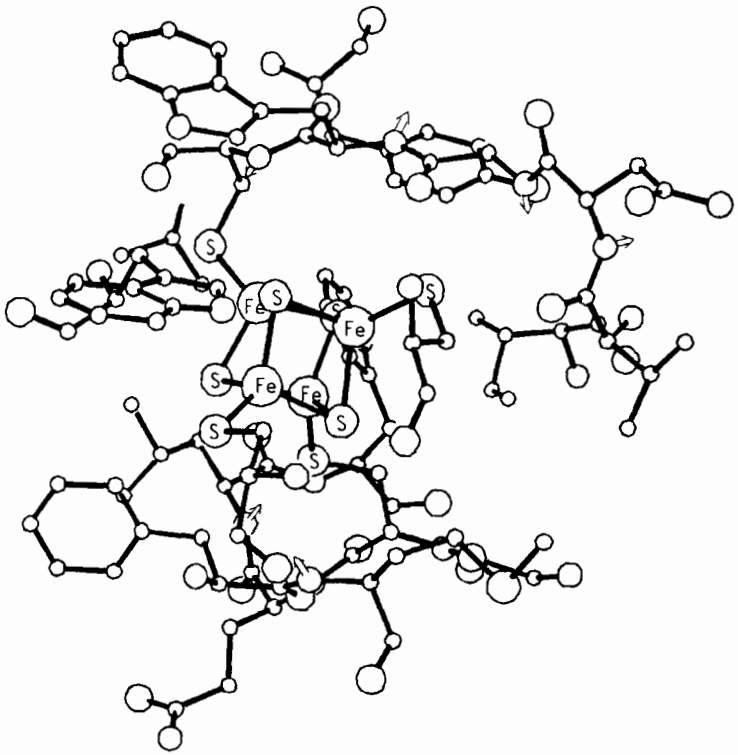

FIG. 16. The crystallographic structure within 5.5 Å of the $Fe_4S_4^{3+}$ core of *Chromatium vinosum* HiPIP (*6*, *53*).

A. Peptide Model and Simple Thiolate Complexes of High-Potential Iron–Sulfur Proteins

The complexes $[Fe_4S_4(Z\text{-cys-Ile-Ala-OMe})_4]^{2-}$ and $[Fe_4S_4(Z\text{-cys-Pro-Val-OMe})_4]^{2-}$, which have a Cys-Ile-Ala sequence and are unlikely therefore to form NH---S hydrogen bonds (see above), exhibit a quasireversible $-2/-1$ redox couple but an irreversible $-3/-2$ couple in DMF. The steric crowding around the Cys thiolate ligand should be associated with the stability of the $[Fe_4S_4(SR)_4]^{1-}$ state, which exists in the oxidized form of a high-potential iron–sulfur protein. The importance of a steric effect was verified by the synthesis of $[Fe_4S_4(2,4,6\text{-trimethylbenzenethiolate})_4]^{2-}$ and $[Fe_4S_4(2,4,6\text{-triisopropylbenzenethiolate})_4]^{2-}$. These complexes exhibit quasireversible redox potentials ($-2/-1$) at $+0.02$ and -0.03 V versus SCE, respectively, in DMF (*54*). The X-ray structural data obtained for $[Fe_4S_4(2,4,6\text{-trimethylbenzenethiolate})_4]^{2-}$ show a relatively long Fe-S(C) bond (2.274 Å) and a narrow Fe–S–C angle (100°), with unusual tortion angles for Fe–S(C) (*55*). These results suggest that the bulky thiolate model complexes possess a somewhat ionic Fe–S character due to decrease of the Fe *d* orbital and S *p* orbital interaction. The fairly stable oxidized form, $[Fe_4S_4(2,4,6\text{-triisopropylbenzenethiolate})_4]^{-}$, was successfully isolated by O'Sullivan and Millar (*56*). Therefore, the ionic character of Fe–S bond stabilizes the oxidized state of the [4Fe–4S] complex. The [4Fe–4S] cluster and thiolate ligands in *Chromatium vinosum* high-potential iron–sulfur protein are located in the middle of a hydrophobic domain and possess one restricted Fe–S(C) torsion angle among other more stabilized Fe–S(C) torsion angles (*53*).

B. Catalysis by Peptide Model Complexes

Recently, aconitase has been proposed to have a unique $Fe_4S_4^{2+}$ core at the active site, as shown in Fig. 17 (*57*). The cluster consists of one reactive Fe ion in one corner of the cubane cluster and three inert Fe ions occupying the three other corners (*42*). The heterogeneity of the $Fe_4S_4^{2+}$ core may be caused by the unusual peptide coordination.

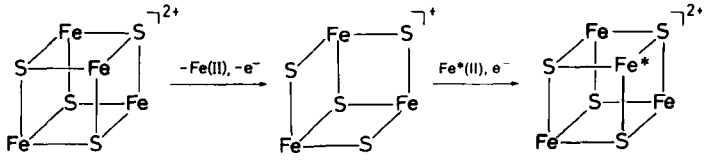

FIG. 17. Interconversion of a [4Fe–4S] cluster to a [4Fe–3S] cluster in the active site of aconitase; Fe* refers to enriched ^{56}Fe and ^{57}Fe (*42*).

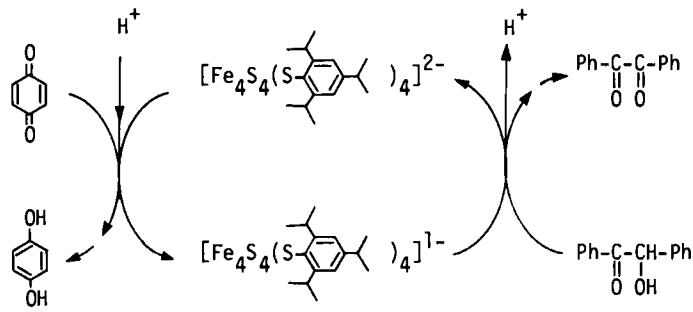

FIG. 18. Catalytic oxidation scheme of benzoin by 1,4-benzoquinone in the presence of $[Fe_4S_4(SR)_4]^{2-}$ in DMF.

Chemical activation of one of the Fe ions for redox reaction has been postulated. The biochemical significance of this type of enzymatic activation should be pursued in the future.

Reductions of acetylene, ketone, isonitrile, or nitrile have been carried out using the $-3/-2$ redox couple of many model complexes (*58–61*), but not using the peptide model complex. A proton transfer function has been observed in studies on the ferredoxin model complex, $[Fe_4S_4(SPh)_4]^{2-}$, in toluene/water (*62*).

A model reaction of oxidation in mitochondria has been proposed using a stable $-2/-1$ redox couple of the bulky thiolate-containing model complexes. Figure 18 shows the scheme of the catalytic oxidation of benzil by benzoquinone in the presence of $Fe_4S_4^{2+}$ complexes (*63*). The complex $[Fe_4S_4(Z\text{-cys-Ile-Ala-OMe})_4]^{2-}$, which has a stable $-2/-1$ redox couple at $+0.12$ V versus SCE in DMF, exhibits a high catalytic activity (*54*).

V. Synthetic Mini-FeS Proteins

Studies aimed at understanding better the functional role of metalloproteins can be classified into at least three distinct categories. In the first case the aim is to synthesize a completely artificial (simple) compound modeling selectively just one of the functions of the metalloprotein, e.g., the picket-fence porphyrin (*64*). Second, from the other extreme, the aim is to modify the protein by substitution of an amino acid residue with another (selected) amino acid residue using recombinant gene technological methods. A third approach is to synthesize a small peptide analog, or "mini-protein," simulating a structural unit in the region containing the active site.

Studies under the latter heading aimed at synthesizing a miniprotein of plant-type ferredoxins have been carried out by Tsukihara *et al.* The procedure has been to obtain a 20-peptide molecule which will have functions similar to those of the ferredoxin when an $Fe_2S_2^{2+}$ core is incorporated (*65*). In the case of *S. platensis* ferredoxin, a major part of the molecule consists of a fairly rigid structure with β barrels. The $Fe_2S_2^{2+}$ core is located in another small domain separated from the major part. A peptide fragment from Pro38 to Ala50 and another fragment from Leu77 to Val80 are combined with a spacer section to give the 20-peptide molecule shown in Fig. 19, which also indicates the expected structure of the 20-peptide/Fe_2S_2 complex. The three procedures, (1) model building (*66*), (2) empirical structure refinement (*67*), and (3) energy minimization by the Levitt method (*68*), have been done successively. The refined structure obtained for the 20-peptide/$Fe_2S_2^{2+}$ complex has no abnormal intramolecular short contacts. The root mean

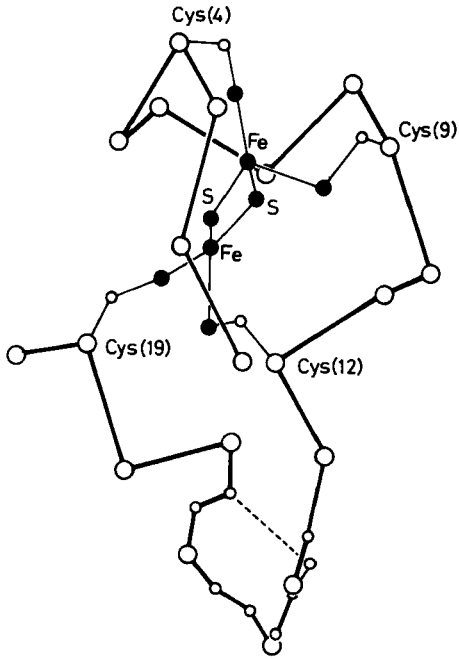

FIG. 19. Schematic structure of the 20-peptide/$Fe_2S_2^{2+}$ complex speculated by the energy minimum calculations (*65*). Large open circles represent α-carbon atoms. Closed circles show Fe(III) and sulfur atoms. Small open circles refer to carbon and nitrogen atoms involved in the artificial hairpin turn and Cys CH_2 carbons. One NH---OC hydrogen bond (dashed line) is expected at the hairpin turn.

square of distances concerned with equivalent atoms are 0.015 and 0.022 nm for the 20-peptide and for the native protein, respectively. The two peptide fragments were connected with a spacer peptide fragment, Gly-Pro-Leu, without large deformation. In this work the water-accessible surface for 2Fe ions was also calculated. The minimum distances are 0.005 and 0.0065 nm for native ferredoxin, while both values for the 20-peptide complex are 0.005 nm. Therefore, the 20-peptide complex can presumably avoid solvent interaction if it can conserve the specified conformation.

The synthetic [2Fe–2S] model complex of the 20-peptide complex exhibits two LMCT absorption maxima at 423 and 461 nm in DMF, maxima which are near to those of the native plant-type ferredoxin (423 and 466 nm) (*69*). Two redox couples for $-3/-2$ were observed at -0.64 V versus SCE and at -0.96 V versus SCE in DMF. One of them is very close to the value (-0.64 V versus SCE) of native ferredoxin. The 20-peptide complex containing invariant sequences Cys-A-B-C-D-Cys-X-Y-Cys and Leu-Thr-Cys-Val possesses all essential factors for a model of the active site except for the peptide conformation. The positive-shifted redox potential of the 20-peptide complex in DMF is undoubtedly due to the interactions between the $Fe_2S_2^{2+}$ core and adjacent amino-acid residues, giving rise to NH---S hydrogen bonding.

VI. Summary

The significance of invariant peptide fragments around the active site of iron–sulfur proteins has been emphasized with respect to their unique ability to modify various chemical properties. In this review, we have considered contributions of such invariant peptide ligands, to, e.g., the shift in redox potentials, to NH---S hydrogen bonding, as well as to hydrophobic environments around the thiolate sulfur atoms. In addition, peptide fragments around the active site could be involved in other significant functions, such as the achievement of low-energy electron transfer reactions. Specific peptides can also serve as mediators for electron passage, and for protection against dioxygen, water, and protons. Many chemical functions are obviously controlled by the specific combination of metal coordination site and surrounding peptide environment.

References

1. Berg, J. M., and Holm, R. H., *in* "Iron-Sulfur Proteins" (T. G. Spiro, ed.), p. 1. Wiley, New York, 1982.
2. Holm, R. H., *Acc. Chem. Res.* **10,** 427 (1977).

3. Mayerler, J. J., Denmark, S. E., DePamphilis, B. V., Ibers, J. A., and Holm, R. H., *J. Am. Chem. Soc.* **97,** 1032 (1975).
4. Eklund, H., Nordström, B., Zeppezauer, E., Söderlund, G., Ohlsson, I., Boiwe, T. L., Sonderberg, B. O., Tapia, O., and Bränden, C. I., *J. Mol. Biol.* **102,** 27 (1976).
5. Monaco, H. L., Crawford, J. L., and Lipscomb, W. N., *Proc. Natl. Acad. Sci. U.S.A.* **75,** 5276 (1978).
6. Taketani, M., Iga, Y., Matsuura, Y., Yasuoka, N., Kakudo, M., and Isomoto, Y., *Proc. Int. CODATA Conf., 7th, 1980,* p. 84 (1981).
7. Nakata, M., Ueyama, N., Fuji, M., Nakamura, A., Wada, K., and Matsubara, H., *Biochim. Biophys. Acta* **788,** 306 (1984).
8. Foulkes, E. C., "Biological Roles of Metallothionein." Elsevier North-Holland, Amsterdam, 1981.
9. Adman, E. T., Sieker, L. C., and Jensen, L. H., *J. Biol. Chem.* **248,** 3987 (1973).
10. Watenpaugh, K. D., Sieker, L. C., and Jensen, L. H., *J. Mol. Biol.* **131,** 509 (1979).
11. Adman, E. T., Sieker, L. C., Jensen, L. H., Bruschi, M., and LeGall, J., *J. Mol. Biol.* **112,** 113 (1977).
12. Lane, R. W., Ibers, J. A., Frankel, R. B., Papaefthymiou, G. C., and Holm, R. H., *J. Am. Chem. Soc.* **99,** 84 (1977).
13. Sugiura, Y., Kunishima, M., and Tanaka, H., *Biochem. Biophys. Res. Commun.* **48,** 1400 (1972); Ali, A., Fahrenholz, F., Faring, J. C., and Weinstein, B., *Int. J. Pept. Protein Res.* **5,** 91 (1973).
14. Cristou, G., Ridge, B., and Rydon, H. N., *J. Chem. Soc., Chem. Commun.* 908 (1977).
15. Que, L., Jr., Anglin, J. R., Bobrik, M. A., Davison, A., and Holm, R. H., *J. Am. Chem. Soc.* **96,** 6042 (1974).
16. Burt, R. J., Ridge, B., and Rydon, H. N., *J. Chem. Soc., Dalton Trans.* 1228 (1980).
17. Millar, M., Lee, J. F., Koch, S. A., and Fikar, R., *Inorg. Chem.* **21,** 4106 (1982).
18. Adman, E. T., *Biochim. Biophys. Acta* **549,** 107 (1979).
19. Orme-Johnson, W. H., *Annu. Rev. Biochem.* **42,** 109 (1973).
20. Ueyama, N., Nakata, M., Fuji, M., Terakawa, T., and Nakamura, A., *Inorg. Chem.* **24,** 2190 (1985).
21. Ueyama, N., Sugawara, T., Tatsumi, K., and Nakamura, A., *Inorg. Chem.* **26,** 1978 (1987).
22. Watenpaugh, K. D., Sieker, L. C., Herriott, J. R., and Jensen, L. H., *Acta Crystallogr., Sect. B* **B29,** 943 (1973).
23. Watenpaugh, K. D., Sieker, L. C., and Jensen, L. H., *J. Mol. Biol.* **138,** 615 (1980).
24. Shulman, R. G., Eisenberger, P., Blumberg, W. E., and Stombaugh, N. A., *Proc. Natl. Acad. Sci. U.S.A.* **72,** 4003 (1975); Sayers, D. E., Stern, E. A., and Herriott, J. R., *J. Chem. Phys.* **64,** 427 (1976).
25. Yachandra, V. K., Hare, J., Moura, I., and Spiro, T. G., *J. Am. Chem. Soc.* **105,** 6455 (1983).
26. Czernuszewicz, R. S., LeGall, J., Moura, I., and Spiro, T. G., *Inorg. Chem.* **25,** 696 (1986).
27. Ueno, S., Ueyama, N., Nakamura, A., and Tsukihara, T., *Inorg. Chem.* **25,** 1000 (1986).
28. Nakata, M., Ueyama, N., Terakawa, T., and Nakamura, A., *Bull. Chem. Soc. Jpn.* **56,** 3647 (1983).
29. Bair, R. A., and Goddard, W. A., III, *J. Am. Chem. Soc.* **100,** 5669 (1978).
30. Tsukihara, T., Fukuyama, K., Tahara, H., Katsube, Y., Matsuura, Y., Tanaka, N., Kakudo, M., Wada, K., and Matsubara, H., *J. Biochem. (Tokyo)* **84,** 1645 (1978).
31. Sanders-Loehr, J., Mino, Y., and Loehr, T. M., *Rect. Trav. Chim. Pays-Bas* 363 (1987).
32. Tagawa, K., and Arnon, D. I., *Biochim. Biophys. Acta* **153,** 602 (1968).
33. Mascharak, P. K., Papaefthymiou, G. C., Frankel, R. B., and Holm, R. H., *J. Am. Chem. Soc.* **103,** 6110 (1981).

34. Ueyama, N., Ueno, S., and Nakamura, A., *Bull. Chem. Soc. Jpn.* **60,** 283 (1987).
35. Ueno, S., Ueyama, N., and Nakamura, A., *Pept. Chem. 1984*, p. 269 (1985).
36. Sweeney, W. V., Rabinowitz, J. C., and Yoch, D. C., *J. Biol. Chem.* **250,** 7842 (1975); Emptage, M. H., Kent, T. A., Huynth, B. H., Rawlings, J., Orme-Johnson, W. H., and Münck, E., *J. Biol. Chem.* **255,** 1793 (1980).
37. Ghosh, D., Furey, W., Jr., O'Donnell, S., and Stout, C. D., *J. Biol. Chem.* **256,** 4185 (1981).
38. Stout, G. H., Turley, S., Sieker, L. C., and Jensen, L. H., *Congr. Gen. Assembly. Int. Union Crystallogr., 14th, 1987.*
39. Antonio, M. R., Averill, B. A., Moura, I., Moura, J. J. G., Orme-Johnson, W. H., Teo, B.-K., and Xavier, A. V., *J. Biol. Chem.* **257,** 8846 (1982); Beinert, H., Emptage, M. H., Dreyer, J.-L., Scott, R. A., Hahn, J. E., Hodgson, K. O., and Thomson, A. J., *Proc. Natl. Acad. Sci. U.S.A.* **80,** 393 (1983).
40. Johnson, M. K., Czernuszewics, R. S., Spiro, T. G., Fee, J. A., and Sweeney, W. V., *J. Am. Chem. Soc.* **105,** 6671 (1983).
41. Nagayama, K., Ohmori, D., Imai, T., and Oshima, T., *FEBS Lett.* **158,** 208 (1983).
42. Kent, T. A., Emptage, M. H., Merkle, H., Kennedy, M. C., Beinert, H., and Münck, E., *J. Biol. Chem.* **260,** 6871 (1985).
43. DePamphilis, B. V., Averill, B. A., Herskovitz, T., Que, L., Jr., and Holm, R. H., *J. Am. Chem. Soc.* **96,** 4159 (1974).
44. Kassner, R. J., and Yang, W., *J. Am. Chem. Soc.* **99,** 4351 (1977).
45. Adman, E., Watenpaugh, K. D., and Jensen, L. H., *Proc. Natl. Acad. Sci. U.S.A.* **72,** 4854 (1975).
46. Sheridan, R. P., Allen, L. C., and Carter, C. W., Jr., *J. Biol. Chem.* **256,** 5052 (1981).
47. Ueyama, N., Terakawa, T., Nakata, M., and Nakamura, A., *J. Am. Chem. Soc.* **105,** 7098 (1983).
48. Warshel, A., *Acc. Chem. Res.* **14,** 284 (1981).
49. Ueyama, N., Kajiwara, A., Terakawa, T., Ueno, S., and Nakamura, A., *Inorg. Chem.* **24,** 4700 (1985).
50. Nieman, J., Naaktgeboren, A. J., and Reedijk, J., *Inorg. Chim. Acta* **L9,** 93 (1984).
51. Ueyama, N., Fuji, M., Sugawara, T., and Nakamura, A., *Pept. Chem. 1984*, p. 301 (1985).
52. Packer, E. L., Sweeney, W. V., Rabinowitz, J. C., Sternlicht, H., and Shaw, E. N., *J. Biol. Chem.* **252,** 2245 (1977).
53. Carter, C. W., Jr., Kraut, J., Freer, S. T., Alden, R. A., Sieker, L. C., Adman, E. T., and Jensen, L. H., *Proc. Natl. Acad. Sci. U.S.A.* **69,** 3526 (1972).
54. Ueyama, N., Terakawa, T., Sugawara, T., Fuji, M., and Nakamura, A., *Chem. Lett.* 1287 (1984).
55. Ueyama, N., Sugawara, T., Fuji, M., Nakamura, A., and Yasuoka, N., *Chem. Lett.* 175 (1985).
56. O'Sullivan, T., and Millar, M. M., *J. Am. Chem. Soc.* **107,** 4096 (1985).
57. Kent, T. A., Dreyer, J.-L., Kennedy, M. C., Huynh, B. H., Emptage, M. H., Beinert H., and Münck, E., *Proc. Natl. Acad. Sci. U.S.A.* **79,** 1096 (1982).
58. Inoue, H., Fujimoto, N., and Imoto, E., *J. Chem. Soc., Chem. Commun.* 412 (1977).
59. McMillan, R. S., Renaud, J., Reynolds, J. G., and Holm, R. H., *J. Inorg. Biochem.* **11,** 213 (1979); Christou, G., Hageman, R. V., and Holm, R. H., *J. Am. Chem. Soc.* **102,** 7600 (1980).
60. Tanaka, K., Imanaka, Y., Tanaka, M., Honjo, T., and Tanaka, T., *J. Am. Chem. Soc.* **104,** 4258 (1982).
61. Okura, I., Nakamura, S., and Kobayashi, M., *Bull. Chem. Soc. Jpn.* **54,** 3794 (1981).
62. Tsai, H., Sweeney, W. V., and Coyle, C. L., *Inorg. Chem.* **24,** 2796 (1985).

63. Ueyama, N., Sugawara, T., Kajiwara, A., and Nakamura, A., *J. Chem. Soc., Chem. Commun.* 434 (1986).
64. Collman, J. P., Gagne, R. R., Halbert, T. R., Marchon, J.-C., and Reed, C., *J. Am. Chem. Soc.* **75,** 5595 (1974).
65. Tsukihara, T., Kobayashi, M., Nakamura, M., Katsube, Y., Fukuyama, K., Hase, T., Wada, K., and Matsubara, H., *BioSystems* **15,** 243 (1982).
66. Diamond, R., *Acta Crystallogr.* **21,** 253 (1966).
67. Hendrickson, W. A., and Konnert, J. H., *in* "Biomolecular Structure, Function, and Evolution" (R. Srinivasan, ed.), Vol. 1, p. 43. Pergamon, Oxford, 1980.
68. Levitt, M., *J. Mol. Biol.* **82,** 393 (1974).
69. Ueno, S., Ueyama, N., Nakamura, A., Wada, K., Matsubara, H., Kumagai, S., Sakakibara, S., and Tsukihara, T., *Pept. Chem. 1983,* p. 133 (1984).